CrystEngComm

Accepted Manuscript

ROYAL SOCIETY OF CHEMISTRY

www.rsc.org/crystengcomm

Effect of Sb_2Se on phase change characteristics of $Ge_2Sb_2Te_5$

Miao Wang,[a] Yegang Lu,*[a] Xiang Shen,[b] ,Guoxiang Wang,[b] Jun Li,[a] Shixun Dai,[b] Sannian Song,[c] and Zhiang Song[c]

Abstract

In this paper, effect of Sb_2Se on phase change characteristics of $Ge_2Sb_2Te_5$(GST) are systemically studied for applications in phase-change random access memory (PRAM). The crystallization temperature of Sb_2Se-GST increases with the increasing Sb_2Se content, while the archival life of amorphous state firstly decreases and then increase. The phase transition from face-centered-cubic (FCC) to hexagonal(HEX) phase was suppressed when Se atomic percentage is larger than 9% for Sb_2Se-GST film. The widen band gap and high value of $B^{1/2}$ lead to about five orders of magnitude of the resistance contrast between amorphous and crystalline states. Compared with GST, $Ge_4Sb_{52}Te_9Se_{35}$ shows high crystallization temperature, wider band gap and a fast switching speed, suggesting a potential candidate for PRAM.

1. Introduction

Phase change memory (PCM) has attracted much attention due to its high speed, excellent scalability and good compatibility with complementary metal-oxide-semiconductor (CMOS) technology [1-3]. PCM utilizes the high resistance contrast between amorphous and crystalline states of phase change material to store information. GST is the most widely used phase change materials for its good comprehensive properties such as good trade-off between crystallization rate and thermal stability. However, there are several issues needed to be addressed for GST scaled down to a smaller dimension which is promising for future generations. High melting temperature (~620℃ for GST) will cause a high RESET current in PCM devices, leading to higher power consumption[4]. Besides, low crystallization temperature(T_c, about 170℃) results in the thermal stability with 10-year data retention temperature at 85℃[5, 6] that is not ideal for the consumer products and automotive systems.

Many efforts are devoted to optimizing the data retention, high speed, and power of GST. Doping is one of the most effective ways to improve the property of PCM. For example, in order to enhance the data retention, many elements such as Ag[7], Al[8], Zn[9], Cu[10], Ti[11], N&O[12] doped into the conventional GST. Especially, SnTe doping GST exhibits a faster crystallization speed than GST[13], which is favorable to the operation speed of PCM. This improvement attributes to a weaker bonding strength of Sn–Te (359.8 kJ·mol^{-1}) compared with the Ge–Te bond (397 kJ·mol^{-1})[13]. Recently, Sb-Se was proposed for low power PCM due to its low thermal conductivity and low melting point[14]. It is shown that Sb_2Se has higher T_c (198℃) and 10-year life time temperature(107℃))[15] than GST，suggesting a better thermal stability for

PCM. In addition, Sb_2Se shows a faster crystallization since Sb-rich phase-change materials have a growth-dominated crystallization behavior rather than a nucleation-dominated one(GST)[16]. From this point of view, Sb_2Se-GST materials will possess the characteristics of better thermal stability as well as faster crystallization speed. Therefore, it is worthwhile to incorporate Sb_2Se into GST and to investigate structural, thermal, optical, and electrical properties.

2. Experimental

Sb_2Se-GST films were deposited on Si/SiO_2 substrate at room temperature via co-sputtering Sb_2Se and GST alloy targets. The background pressure was 1.6^{-4} Pa, and chamber pressure became 0.3 Pa during the film deposition. The dc power on the Sb_2Se target ranged from 3 to 13 W, while the RF power on the GST target ranged from 5 to 50 W for optimizing Sb_2Se content. The composition of the film was determined by energy dispersive spectroscopy (EDS). The samples in this study can be denoted by $Ge_{25}Sb_{23}Te_{50}Se_2$, $Ge_{21}Sb_{29}Te_{41}Se_9$, $Ge_{16}Sb_{36}Te_{29}Se_{19}$ and $Ge_4Sb_{52}Te_9Se_{35}$.The phase structures of the Sb_2Se doping GST thin films were analyzed by the x-ray diffraction (XRD) technique (Bruker D2 PHASER diffractometer) in the 2θ range from 10° to 60°. The sheet resistance of the Sb_2Se-GST film was in situ measured using a four-point probe in a homemade vacuum chamber. The optical transmission in the spectral range 300–2500 nm was obtained by a Perkin-Elmer Lambda 950 UV–VIS–NIR spectrophotometer. The absorption coefficient (α) was calculated by a general relationship:

$$a = -(1/d)ln(T), \quad (1)$$

where d and T are the thickness of the film and transmission, respectively. The optical band gap (E_{opt}) is deduced from the expression:

$$\alpha(v) \cdot hv = B(hv - E_{opt})^2 \text{ [17]}, \quad (2)$$

where B and hv are a constant and the energy of the incident photon, respectively. Raman spectroscopy was employed to study the changes in chemical bonds of Sb_2Se-GST film. The microstructure was analyzed by transmission electron microscope (TEM).

3. Results and discussion

The sheet resistance versus temperature (*R-T*) at a heating rate of 40℃/min for different samples is shown in Fig. 1(a). The resistance of all the films initially decreases slowly with the increasing temperature due to the heat active carrier for hopping conduction. The resistance decreases suddenly to over one order of magnitude when the amorphous-to-crystalline transition occurs. A steep decrease of resistance around the crystallization temperature can be observed for the Sb_2Se-doped GST films. The crystallization temperature (T_c) was determined from the minimum of the derivative of *R-T* curve. T_cs of $Ge_{25}Sb_{23}Te_{50}Se_2$, $Ge_{21}Sb_{29}Te_{41}Se_9$, $Ge_{16}Sb_{36}Te_{29}Se_{19}$ and $Ge_4Sb_{52}Te_9Se_{35}$ are listed in Table 1, which is higher than that of GST(about 170℃). The addition of Sb_2Se will form the nano-mixture phase which brings a larger number of extra bonds into the GST. And it will cause a disturbance to the crystallization behavior of the whole system. Thus, T_c of Sb_2Se-GST film increases with the concentration of Sb_2Se. The slope of *R-T* curve around T_c reflects on the crystallization speed of phase change material which is the crucial factor for the operation speed of PCM. It is shown that the absolute value of slope becomes smaller with increasing Sb_2Se concentration when Se atomic percentage is less than 19%, suggesting the sluggish crystallization of GST with a certain amount of Sb_2Se. As the Se atomic percentage increase to 35%, the absolute value of slope achieves maximum and

the resistance drop become the fastest, as shown in Fig. 1(a). From this point of view, the $Ge_4Sb_{52}Te_9Se_{35}$ has the shortest crystallization time among studied compositions as well as GST. It is noted that resistance undergoes the second drop to a more stable low level for $Ge_{25}Sb_{23}Te_{50}Se_2$ and GST due to the second structure transition. And the transition was suppressed when Se atomic percentage is larger than 9%. For all compositions, about five orders of magnitude of the resistance contrast between amorphous state and crystalline state is helpful in achieving a high On/OFF ratio[18].

Table 1 the crystallization parameters of Ge-Sb-Te-Se films

Composition(at.%)				T_c(°C)	E_a(eV)
Ge	Sb	Te	Se		
25	23	50	2	76	2.31
21	29	41	9	58	1.77
16	36	29	19	101	2.78
4	52	9	35	100	2.54

Thermal stability of as-deposited amorphous is an important factor to forecast the data retention of PCM devices. The failure time is defined as the time when the resistance decrease to half of its initial value at a specific temperature[19]. The data retention of as deposited amorphous film is obtained by the Arrhenius equation[20]:

$$t = Aexp\left[\frac{E_\alpha}{K_bT}\right], \quad (3)$$

where t, A, E_α and K_b are the failure time, a proportional time constant, the activation energy for crystallization and Boltzmann's constant, respectively. The Arrhenius plot of 10-year data retention for as-deposited amorphous Sb_2Se-GST films is given by Fig. 1(b). It is shown that $Ge_{25}Sb_{23}Te_{50}Se_2$ and $Ge_{21}Sb_{29}Te_{41}Se_9$ have poor 10-year data retention capability (below 76℃) in

Fig. 1(b), which is not satisfied for use in PCM device. The data retention can be improved by the Se atomic percentage is larger than 9% which possesses 10-year data retention at above 100℃ as well as a large activation energy for crystallization (above 2.54eV), as shown in Fig. 1(b). Apparently, Sb_2Se-GST film with Se atomic percentage is above 9% owing better thermal stability and larger crystallization activation energy that are more suitable for PCM devices.

The crystalline structure of Sb_2Se-GST films were studied by x-ray diffraction measurement. There are two weak diffraction peaks for $Ge_{25}Sb_{23}Te_{50}Se_2$ and $Ge_{21}Sb_{29}Te_{41}Se_9$ films annealed at 170℃, as shown in Fig. 2(a). This phenomenon can be explained by the low T_c of them. The characteristic peaks appear for $Ge_{16}Sb_{36}Te_{29}Se_{19}$ and $Ge_4Sb_{52}Te_9Se_{35}$ film annealed at 200℃(see Fig. 1(b), suggesting both of them being crystallized. T_cs are about 200℃, which is consistent with *R-T* results. It is also shown that $Ge_4Sb_{52}Te_9Se_{35}$ crystallizes into Sb_2Se_3, Sb and GST phase exhibiting a single FCC GST structure. At 260℃, $Ge_4Sb_{52}Te_9Se_{35}$ exhibits stronger diffraction intensity than other samples, as shown in Fig. 2(c), suggesting its higher degree of crystallinity. The fine crystallinity in the film is related to the low disorder level which leads to high carrier density as a result of more delocalized electronic states. That is why the resistance of $Ge_4Sb_{52}Te_9Se_{35}$ film is lower than those of other compositions at 260℃(see Fig 1(a)). With the annealing temperature increasing to 350℃, the crystalline structure of $Ge_{25}Sb_{23}Te_{50}Se_2$ film transferred from FCC into hexagonal phase, as shown in Fig. 2(d). It is in good agreement with the second-step resistance of $Ge_{25}Sb_{23}Te_{50}Se_2$ film in *R-T* curve. The FCC and hexagonal phases coexists in $Ge_{21}Sb_{29}Te_{41}Se_9$ film at 350℃. As the Se atomic percentage increased to 19%, the precipitation of Sb_2Se_3, Sb, and GST crystalline phases is observed at 350℃, as shown in Fig.

1(d). According to the Scherrer's equatioin[21] the mean crystallite size is inversely proportional to the full width at half maximum (FWHM) of the diffraction peak. It is clearly observed that the FWHM of the peak with maximum intensity increases with the concentration of Sb_2Se, suggesting the addition of Sb_2Se suppressing the grain growth. The $Ge_4Sb_{52}Te_9Se_{35}$ has the minimum crystallite size, which will produce more grain boundaries. As a result, it has relatively high resistance at 350℃(see Fig. 1(a)) due to more carrier scatters compared to other samples.

The spectroscopic ellipsometer can be used to determine E_{opt} of the materials. Transmission spectra and plot of $(\alpha h\nu)^{\frac{1}{2}}$ versus $h\nu$ are for amorphous $Ge_4Sb_{52}Te_9Se_{35}$ film. For higher values ($\alpha>10^4$ cm^{-1}), the absorption coefficient α yields the power part which obeys the Tauc et al[22] and Davis and Mott relation[23, 24] for the allowed indirect transition:

$$(\alpha h\nu)^{\frac{1}{2}} = B^{\frac{1}{2}}(h\nu - E_{opt}), \quad (4)$$

where $B^{\frac{1}{2}}$, h, ν and E_{opt} are a Tauc parameter of the investigated substance, Plank's constant, frequency and the optical band gap, respectively. As shown in Fig. 3, the E_{opt} and slope quantities $B^{1/2}$ of amorphous $Ge_4Sb_{52}Te_9Se_{35}$ film calculated from the Tauc's plot are 0.71eV and 796.4$cm^{-1/2}eV^{-1/2}$, which are higher than those of GST (0.69eV and 714.6 $cm^{-1/2}eV^{-1/2}$)[25]. The widening of band gap in amorphous materials has fundamental importance due to the presence of trap states, which plays an important role in switching by filling up the charge carriers to become conductive [26]. At the same time, a higher value of $B^{1/2}$ indicates more disorder, and consequently increase On/OFF ratio[27]. It indicates the addition of amounts of Sb_2Se into GST is favorable to enhance the switching properties.

The vibration mode of bonds in crystalline phase was analyzed using Raman spectroscopy.

Fig. 4(a) shows Raman spectra of GST and $Ge_4Sb_{52}Te_9Se_{35}$ films annealed at 200℃ . For GST film, the broad Raman band centered at 105 cm^{-1} is associated with the A_1 mode of $GeTe_4$ corner-sharing tetrahedral and a broad band at 155 cm^{-1} is related to Sb–Te bonds' vibrations in $SbTe_3$ units[28]. The main feature of the Raman spectrum for the crystallized $Ge_4Sb_{52}Te_9Se_{35}$ is the existence of two overlapping band with two peaks at about 143 and 163cm^{-1}, which are believed to originate from the $SbTe_3$ pyramids vibrational modes and Sb-Sb bonds vibration modes of [Sb_2Se-$SbSe_2$], respectively. As the annealing temperature increases to 350℃, the Raman spectrum of both samples changed more or less, as shown in Fig. 4(b). The original peak at 163cm^{-1} shifted to higher frequency (about 171cm^{-1}), and the other peak remained its position for GST film. It is indicated that the FCC-to-HEX phase transition of GST is ascribed to the atomic arrangement in $SbTe_3$ units rather than $GeTe_4$ tetrahedral. For $Ge_4Sb_{52}Te_9Se_{35}$ film, the position of peaks keeps motionless and substantial amplitude increases for the peak at 155 cm^{-1} due to the high degree of crystallization. It is suggested that the Sb_2Se phase suppressed significantly the second phase-transition of GST phase for $Ge_4Sb_{52}Te_9Se_{35}$ film, which is good agreement with XRD result.

The bond environment of $Ge_4Sb_{52}Te_9Se_{35}$ film was investigated by X-ray photoelectron spectroscopy. The core level spectra of Se 3d, Sb 3d and Te 3d are plotted in Fig. 5(a)-5(c). The binding energy of Se 3d for $Ge_4Sb_{52}Te_9Se_{35}$ results from Sb-Se peak centered at 53.9eV[29] which is lower than Se-Se homopolar binding energy of pure Se. After Sb_2Se doping into GST, the peak positions of both Sb 3d and Te 3d spectra shift to higher binding energy for $Ge_4Sb_{52}Te_9Se_{35}$ compared with GST, As shown in figure 5(b) and 5(c). It has been reported that

the binding energy of an element increases with increasing electronegative of neighbor bonding atom [6, 30]. The electronegativity of Se, Te, Sb and Ge are 2.55, 2.1, 2.05 and 2.01 respectively[31]. Therefore, Se has formed the chemical bonds with others. It indicates that the incorporation of Sb_2Se into GST suffers from atomic reconfiguration to change the bonding state. The bonding recombination may account for the suppression of the phase transformation from FCC to hexagonal as shown in Fig. 2(d).

The microstructure of $Ge_4Sb_{52}Te_9Se_{35}$ was observed by TEM. The samples were fabricated on carbon membrane substrates. TEM image of $Ge_4Sb_{52}Te_9Se_{35}$ film annealed at 260℃. The black particles with a size of several tens of nanometers are uniformly distributed in the film in Fig. 6(a). The dispersive dots along diffraction ring can be observed in the selected area electron diffraction (SAED) pattern (see Fig. 6 (b)), suggesting high degree of crystallization. Figure 6(c) shows the high-resolution TEM image of $Ge_4Sb_{52}Te_9Se_{35}$ film. The main feature of the black particles was confirmed to be the polycrystalline structure of embedded Sb_2Se, Sb and GST crystallites. The polycrystalline morphology composed of a large number of crystallites with different size smaller than 60 nm, which is characteristic of the nucleation dominated mechanism. There are main two crucial factors to influence the crystalline speed for nucleation dominated mechanism. One is the large nucleation probability which will increase the number of crystal nuclei to promote the fast crystallization. The large differences in electronegativity of $Ge_4Sb_{52}Te_9Se_{35}$ may serves as a nucleation drive to increase the nucleation probability. The other is the small grain size. Compared with the large grain, it will shorten time when nuclei just grow up to a small grain to complete crystallization. Thus, $Ge_4Sb_{52}Te_9Se_{35}$ shows fast crystallization

velocity.

4. Conclusions

In summary, phase change properties of Sb_2Se-GST film were systematically studied. The crystallization temperature of Sb_2Se-GST increases with increasing Sb_2Se content. The data retention ability of amorphous Sb_2Se-GST film can be improved when with the Se atomic percentage is larger than 19%. Only single crystalline phase of FCC could be observed upon annealing for Sb_2Se-GST film with Se atomic percentage larger than 9%. The large resistivity of the crystalline Sb_2Se-GST film is beneficial to reduce the write current. Compared with GST, $Ge_4Sb_{52}Te_9Se_{35}$ film shows better thermal stability, wider band gap and faster crystallization, suggesting a potential candidate for PRAM.

Acknowledgements

This work was supported by the National Natural Science Foundation of China (Grant Nos. 61306147 and 61377061), Ningbo municipal Natural Science Foundation of China (Grant No. 2014A610121), and Natural Science Foundation of Zhejiang Province, China (Grant No. LQ15F040002), and sponsored by K. C. Wong Magna Fund in Ningbo University.

Notes and references

[a]Faculty of Information Science and Engineering, Ningbo University, Zhejiang, 315211

[b]Laboratory of Infrared Material and Devices, The Advanced Technology Research Institute, Ningbo University , Zhejiang, 315211

[c]State Key Laboratory of Functional Materials for Informatics, Shanghai Institute of Micro-system and Information Technology, Chinese Academy of Sciences, Shanghai 200050, People's Republic of China

1. Matsunaga, T. and N. Yamada, Physical Review B, 2004, **69**, 104111.
2. Feng Rao, Zhitang Song, Kun Ren, Xilin Zhou, Yan Cheng, Liangcai Wu and Bo Liu, Nanotechnology, 2011, **22**, 145702.
3. Takahiro Morikawa, Kenzo Kurotsuchi, Yoshihisa Fujisaki, Yuichi Matsui and Norikatsu Takaura, Japanese Journal of Applied Physics, 2012, **51**, 031201.
4. Y. Sutou, T. Kamada, M. Sumiya, Y. Saito, J. KoikeSutou, Acta Materialia, 2012, **60**, 872.
5. Noboru Yamada, Eiji Ohno, Kenichi Nishiuchi, Nobuo Akahira and Masatoshi Takao, Journal of Applied Physics, 1991, **69**, 2849.
6. Min Zhu, Liangcai Wu, Zhitang Song, Feng Rao, Daolin Cai, Cheng Peng, Xilin Zhou, Kun Ren, Sannian Song, Bo liu and Songlin Feng, Applied Physics Letters, 2012, **100**, 122101.
7. Ki-Ho Song, Sung-Won Kim, Jae-Hee Seo, Hyun-Yong Lee, Thin Solid Films, 2009, **517**,

3958.

8. Seo, J.-H., K.-H. Song, and H.-Y. Lee, Journal of Applied Physics, 2010, **108**, 064515.

9. Guoxiang Wang, Qiuhua Nie, Xiang Shen, R. P. Wang, Liangcai Wu, Jing Fu, Tiefeng Xu and Shixun Dai, Applied Physics Letters, 2012, **101**, 051906.

10. Keyuan Ding, Kun Ren, Feng Rao, Zhitang Song, Liangcai Wu, Bo Liu, Songlin Feng, Materials Letters, 2014, **125**, 143.

11. S. J. Wei, H. F. Zhu, K. Chen, D. Xu, J. Li, F. X. Gan, X. Zhang, Y. J. Xia and G. H. Li, Applied Physics Letters, 2011, **98**, 231910.

12. Privitera, S., E. Rimini, and R. Zonca, Applied physics letters, 2004, **85**, 3044.

13. Jian'an Xu, Feng Rao, Zhitang Song, MengJiao Xia, Cheng Peng, Yifeng Gu, Min Zhu, Liangcai Wu, Bo Liu and Songlin Feng, Electrochemical and Solid-State Letters, 2011, **15**, H59.

14. Sung-Min Yoon, Nam-Yeal Lee, Sang-Ouk Ryu, Kyu-Jeong Choi, Young-Sam Park, Seung-Yun Lee, Byoung-Gon Yu, Myung-Jin Kang, Se-Young Choi, and Matthis Wuttig, Electron Device Letters, IEEE, 2006, **27**, 445.

15. Yifeng Hu, Simian Li, Tianshu Lai, Sannian Song, Zhitang Song, Jiwei Zhai, Scripta Materialia, 2013, **69**, 61.

16. Yegang Lu, Sannian Song, Zhitang Song and Bo Liu, Journal of Applied Physics, 2011, **109**, 064503.

17. Feng Rao, Zhitang Song, Yan Cheng, Mengjiao Xia, Kun Ren, Liangcai Wu, Bo Liu, Songlin Feng, Acta Materialia, 2012, **60**, 323.

18. Changzhou Wang, Simian Li, Jiwei Zhai , Bo Shen, Mingcheng Sun, Tianshu Lai, Scripta Materialia, 2011, **64**, 645.

19. Kin-Fu Kao, Chain-Ming Lee, Ming-Jung Chen, Ming-Jinn Tsai, Tsung-Shune Chin, Advanced Materials, 2009, **21**, 1695.

20. Yifeng Hu, Mingcheng Sun, Sannian Song, Zhitang Song, Jiwei Zhai, Integrated Ferroelectrics, 2012, **140**, 8.

21. Yin, Y., H. Sone, and S. Hosaka, Japanese journal of applied physics, 2005, **44**, 6208.

22. Davis, E. and N. Mott, Philosophical Magazine, 1970, **22**, 0903.

23. Parvanov, S., V. Vassilev, and K. Tomova, Materials Letters, 2008, **62**, 2021.

24. Bong-Sub Lee, John R. Abelson, Stephen G. Bishop, Dae-Hwan Kang, Byung-ki Cheong and Ki-Bum Kim, Journal of Applied Physics, 2005, **97**, 093509.

25. Ki-Ho Song, Sung-Won Kim, Jae-Hee Seo, and Hyun-Yong Lee, Journal of Applied Physics, 2008, **104**, 103516.

26. Wojciech We nic, Ariesto Pamungkas, Ralf Detemple, Christoph Steimer, Stefan Blügel & Matthias Wuttig, Nature Materials, 2006, **5**, 56.

27. Zanatta, A. and I. Chambouleyron, Physical Review B, 1996, **53**, 3833.

28. P. Němec, A. Moreac, V. Nazabal, M. Pavlišta, J. Přikry and M. Frumar, Journal of Applied Physics, 2009, **106**, 103509.

29. Guozhen Shen, Di Chen, Kaibin Tang, Xuan Jiang, Yitai Qian, Journal of Crystal Growth, 2003, **252**, 350.

30. Liu Bo, Song Zhi-Tang, Zhang Ting, Feng Song-Lin and Chen Bomy, Chinese Physics,

2004, **13**, 1947.

31. E. M. Vinod, K. Ramesh, and K. S. Sangunni, Scientific reports, 2015, **5**, 8050.

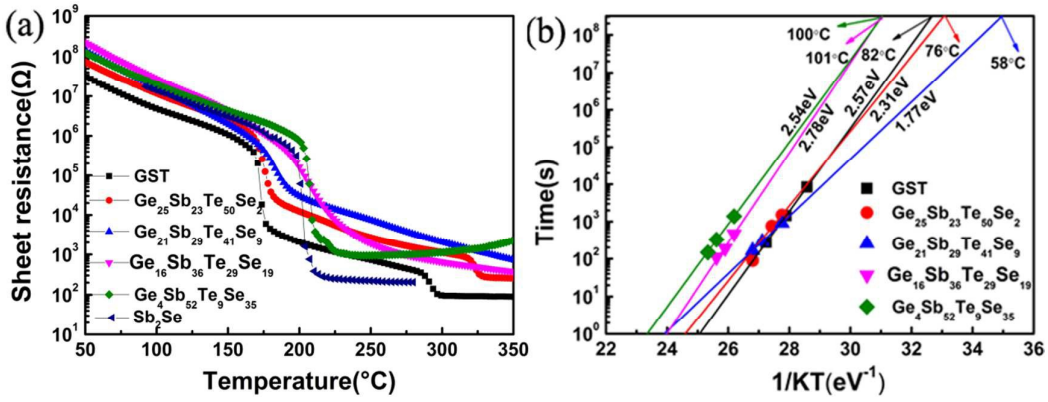

FIG.1. (a) Sheet resistance as a function of temperature for pure and Sb_2Se-doped GST films. (b) Failure time versus reciprocal temperature for Sb_2Se-doped GST films.

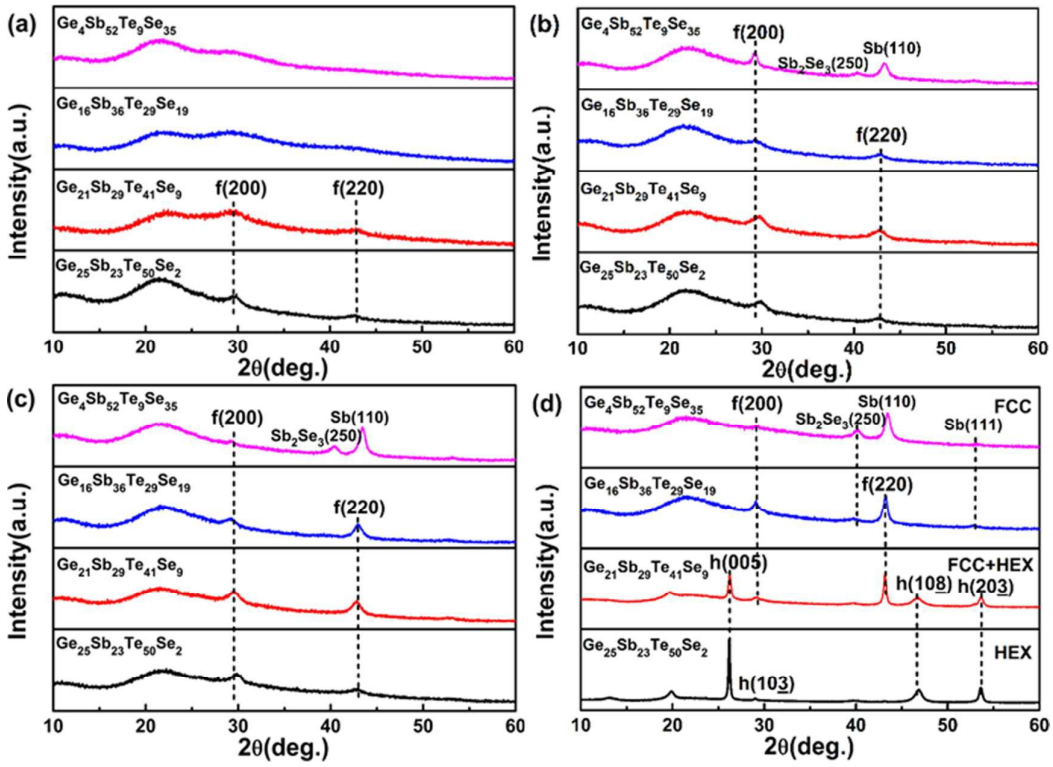

FIG.2. XRD patterns of Sb_2Se-GST films (a) 170℃, (b) 200℃, (c) 260℃, and (d) 350℃, respectively.

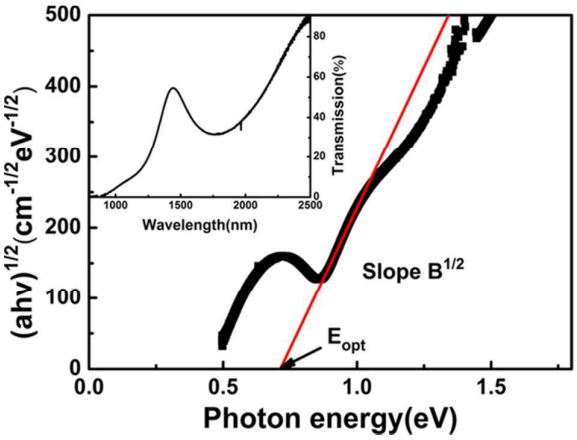

FIG.3. Plots of $(ahv^{1/2})$ vs hv for as deposited $Ge_4Sb_{52}Te_9Se_{35}$ film; Inset shows Vis-IR transmission spectra.

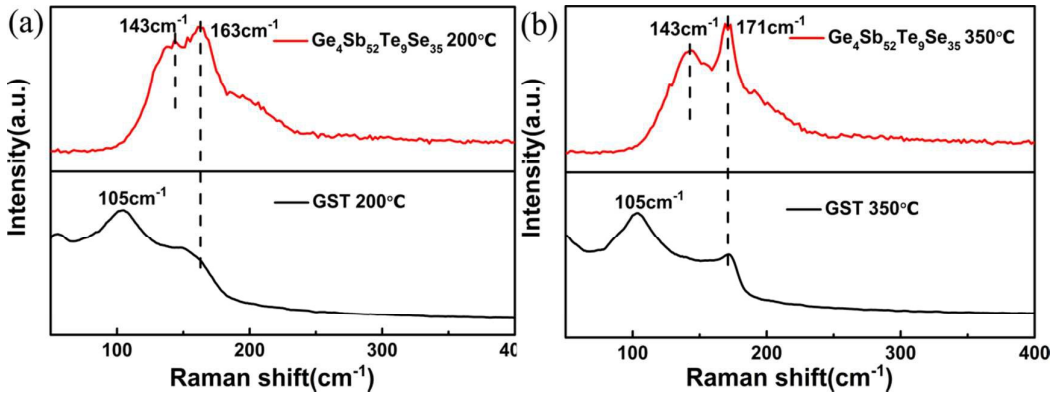

FIG.4. Raman spectra of GST and $Ge_4Sb_{52}Te_9Se_{35}$ films annealed at (a) 200℃ and (b) 350℃.

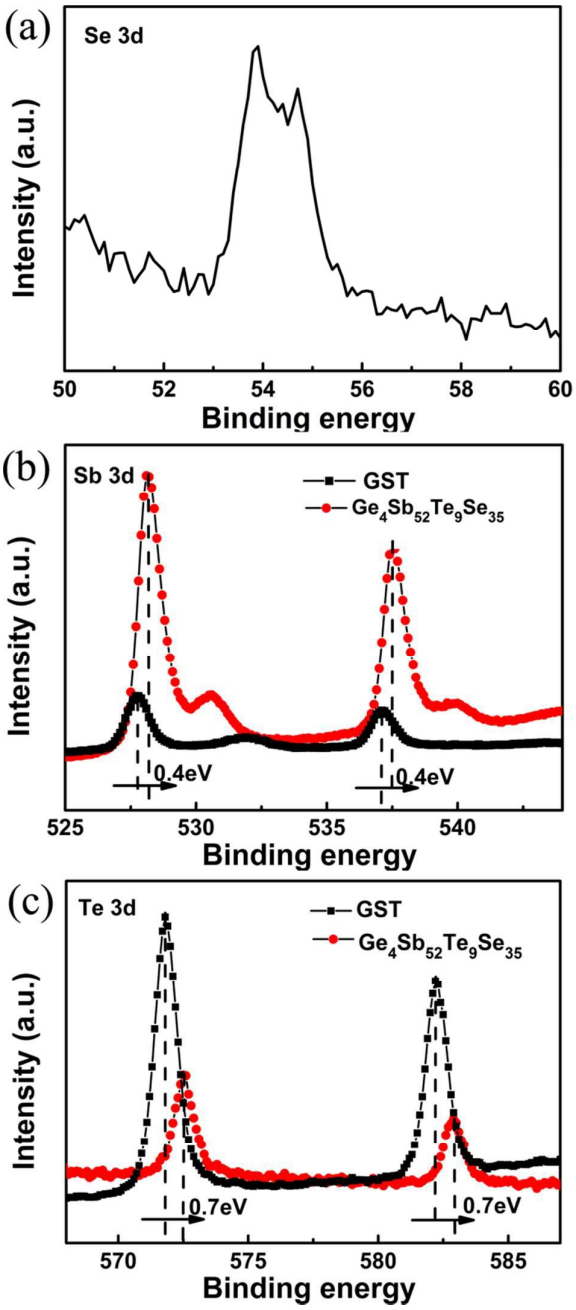

FIG.5. XPS spectra for crystalline GST and $Ge_4Sb_{52}Te_9Se_{35}$ films: (a) Se 3d, (b) Sb 3d, and (c) Te 3d.

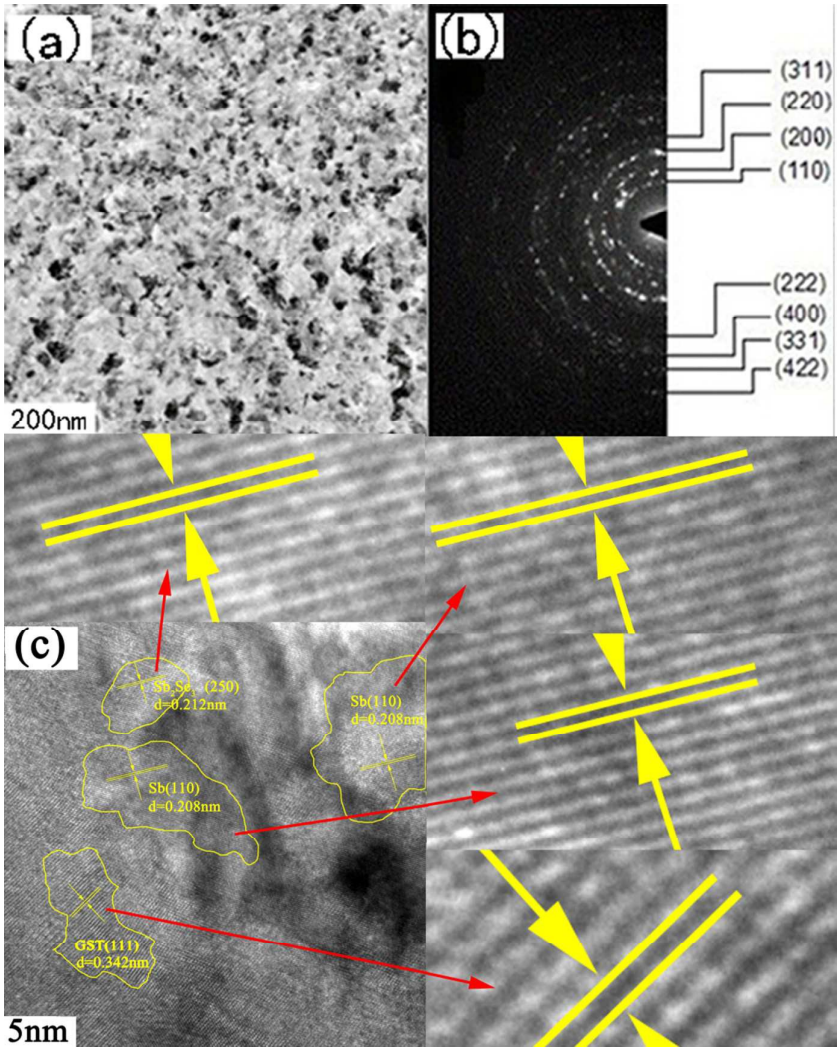

FIG.6. (a) TEM, (b) SAED pattern and (c) HRTEM of $Ge_4Sb_{52}Te_9Se_{35}$ film annealed at 260℃, respectively.

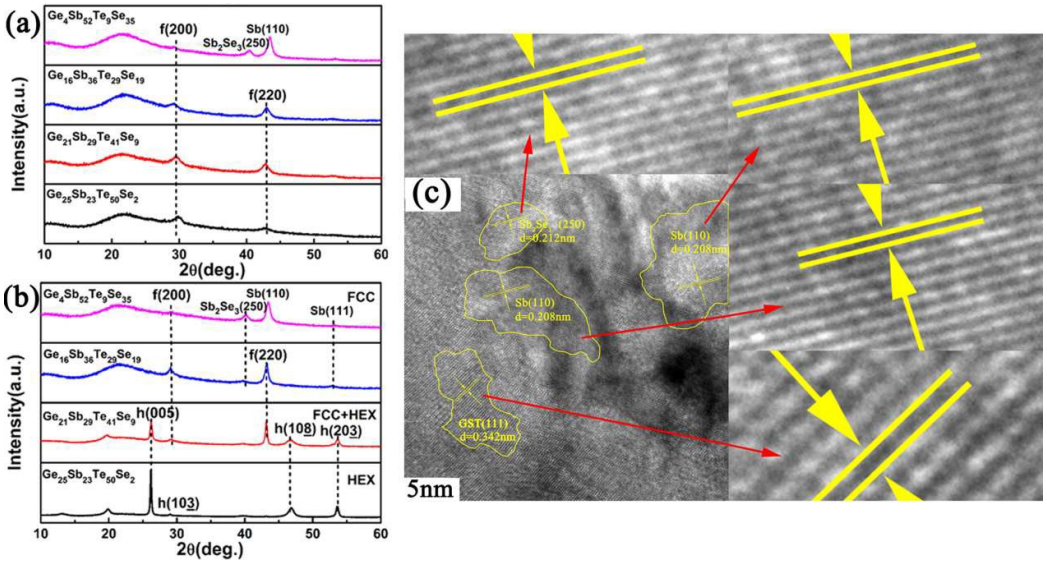

$Ge_4Sb_{52}Te_9Se_{35}$ exhibits stronger diffraction intensity than other samples, as shown in Fig. (a), suggesting its higher degree of crystallinity. The fine crystallinity in the film is related to the low disorder level which leads to high carrier density as a result of more delocalized electronic states. As the Se atomic percentage increased to 19%, the precipitation of Sb_2Se_3, Sb, and GST crystalline phases is observed at 350℃, as shown in Fig. (b). And the phase transition from face-centered-cubic to hexagonal phase was suppressed. The main feature of the black particles was confirmed to be the polycrystalline structure of embedded Sb_2Se, Sb and GST crystallites as shown in Fig. (c). The polycrystalline morphology composed of a large number of crystallites with different size smaller than 60 nm. Compared with the large grain, it will shorten time when nuclei just grow up to a small grain to complete crystallization. Thus, $Ge_4Sb_{52}Te_9Se_{35}$ shows fast crystallization velocity.